ELSEVIER

Journal of Fluids and Structures 26 (2010) 1034–1041

JOURNAL OF FLUIDS AND STRUCTURES

www.elsevier.com/locate/jfs

Special Brief Communication

Scaling of flow separation on a pitching low aspect ratio plate

T. Yilmaz[a], M. Ol[b], D. Rockwell[a,*]

[a]*Department of Mechanical Engineering and Mechanics, Lehigh University, Bethlehem, PA 18015, USA*
[b]*US Air Force Research Laboratory, Air Vehicles Directorate, Wright-Patterson AFB, OH 45433-7542, USA*

Received 28 April 2010; accepted 24 July 2010

Abstract

We use two different dye injection approaches, in two different water tunnels, to visualize the formation and subsequent evolution of leading-edge vortices and related separated structures, for a pitching low aspect ratio plate. The motion is a smoothed linear pitch ramp from 0° to 40° incidence, brief hold, and return to 0°, executed at reduced pitch rates ranging from 0.1 to 0.35 and about various pivot locations. All cases evince a leading edge vortex with pronounced axial flow, which leads to formation of large-scale, three-dimensional flow structures, culminating in a large vortical structure centered at the wing symmetry plane. Pitch is also compared to plunge, where the plunge-induced angle of attack is taken as the geometric pitch incidence angle, ignoring pitch-rate effects. At successively increasing values of convective time C/U, the three-dimensional patterns of the flow structure are remarkably similar for the pitching and plunging motions. The similarity of these patterns persists, though they are shifted in time, for variation of either the location of the pitching axis or the dimensionless pitch rate.

Keywords: Aerodynamics; Unsteady flow; Vortices; Flow–structure interaction; Separated flows; Visualization

1. Introduction

The flow structure and evolution of aerodynamic forces on wings undergoing various abstracted unsteady motions have been of major interest in recent years, primarily from a two-dimensional perspective, and substantial insight has been gained from these investigations. Less attention has been devoted to the three-dimensional aspects, and most such work has focused on the wake structure. Our present interest is therefore the three-dimensional flowfield on the suction side of a low aspect ratio plate in pitch and plunge.

Freymuth (1989) used smoke visualization to describe three-dimensional patterns of the wake downstream of a pitching airfoil. More recently, Von Ellenrieder et al. (2003) and Parker et al. (2005, 2007) considered the case of a heaving–pitching airfoil, and characterized the structure of the near wake. Buchholz and Smits (2006, 2008) determined the topology of the wake of a plate undergoing pitching motion about its leading edge. These experimental studies are complemented by computations of the near-wake vortex structure by Blondeaux et al. (2005) and Dong et al. (2006) for airfoils/plates in periodic motion. For plates subjected to impulsive translation, Taira and Colonius (2009a, b) computed the wake structure, and defined the interaction between the tip and trailing-edge vortices.

*Corresponding author.
E-mail address: dor0@lehigh.edu (D. Rockwell).

0889-9746/$ - see front matter © 2010 Elsevier Ltd. All rights reserved.
doi:10.1016/j.jfluidstructs.2010.07.003

While the foregoing studies concentrated on the structure of the near wake of an airfoil/wing/plate in unsteady motion, the present investigation addresses the three-dimensional flow structure on the suction side of a finite span wing. Due to wingtip effects, generation of three-dimensional flow structure along the span is expected to occur. It is therefore relevant to consider previous studies of development of vortices in the presence of end effects. Kurosaka et al. (1988) and Koochesfahani (1989) observed, respectively, axial flow in vortices within a separated shear layer bounded by a solid wall, and the vortices generated from an oscillating airfoil bounded by end walls. Cohn and Koochesfahani (1993) further demonstrated that a free slip boundary could induce axial flow in a shed vortex. Visbal et al. (1998), in a combined computational–experimental investigation of a planar wall jet subjected to controlled forcing, showed that substantial axial flow could be generated in nominally two-dimensional spanwise vortices, irrespective of whether the ends of the plate were terminated by a wall or a free boundary. In addition, they defined the detailed flow structure during sequential stages of development of the three-dimensional vortices.

Graham and Yeow (1990) considered a nominally two-dimensional NACA 0015 airfoil in linear pitch ramp–return motions in a water tunnel, finding an increase in lift coefficient and tightening of the leading edge vortex structure with increasing reduced frequency of motion. Here we consider a similar motion for an aspect ratio 2 plate, with emphasis on combining three-dimensional qualitative observations, moderately high-rate high-amplitude motions, and a low aspect ratio configuration, to seek a relationship between motion kinematics and the scaling of flow separation over the plate's suction side.

The consequences of finite aspect ratio for a plate in periodic sinusoidal plunge are described in the recent investigation of Yilmaz and Rockwell (2010). Formation of the leading-edge vortex involved pronounced axial flow from each wingtip towards the plane of symmetry, and the subsequent interaction of these axial flows yielded a large-scale, three-dimensional, streamwise-oriented vortical structure. Major unclarified issues include the degree to which pronounced axial flow through leading-edge vortices, culminating in large-scale three-dimensional vortical structures, persists for transient as opposed to sustained periodic motion of the wing over a large number of cycles; different modes of motion of the wing, i.e., pitching versus plunging; variation of location of the pitch pivot point, or pitching axis; and changes of the dimensionless pitch rate. We address these aspects and seek to determine whether an overarching similarity of development of the vortex structure exists.

2. Experimental methods

Experiments were performed in free surface water tunnel facilities at the Lehigh University and the US Air Force Research Laboratory. Details of these facilities and the associated wing motion rigs are given by Yilmaz and Rockwell (2010) and Ol et al. (2005), respectively. Both used an aspect ratio 2.0 rectangular flat plate with all edges of nominally semicircular contour. A schematic of the wing and definition of related parameters are given in Fig. 1(a).

The facility at the Lehigh University had a test-section 508 mm deep and 613 mm wide, and for the present experiments, was operated in the range of free-stream velocity of $U = 45$–90 mm/s, with a turbulence intensity of 0.2%. The wing had a total span $b = 203.2$ mm, chord $C = 101.6$ mm, and thickness $t = 1.59$ mm. Maximum blockage based on wing streamwise projected area was 4.3% at 40° incidence. The plate was supported by a vertical sting in the form of a thin plate of chordwise length of $0.27C$ and a thickness of $0.019b$. The sting was attached to the plate at its mid-span and mid-chord location. Pitching motion was achieved by a small chain of thickness $0.019b$ about the periphery of the

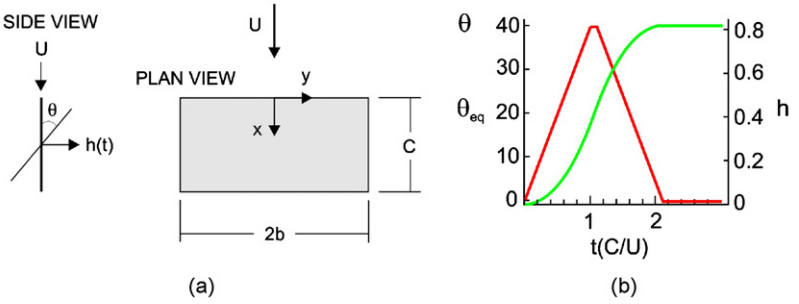

Fig. 1. (a) Schematic of wing (rectangular flat plate) and associated terminology; (b) variation of angle of attack θ of pitching motion, equivalent angle of attack θ_{eq} of plunging motion, and displacement h of plunging motion, which has been normalized by the chord C. Pitching motion corresponds to $K = 0.35$.

sting plate, and connected to a computer-controlled motor at the top of the sting. Simultaneous horizontal and vertical translations were achieved by computer-controlled traverse tables. An arbitrary streamwise location of the pitch pivot point could therefore be prescribed. Dye (35% blue food coloring and 65% water) was gravity-fed from a single plastic tube connected to the wing surface, then through six channels within the wing. Dye ports of diameter 1 mm were drilled into the leeward side of the wing at spanwise locations ± 48, ± 96, and ± 100.6 mm measured from the plane of symmetry of the wing. These locations correspond, respectively, to distances from the plane of symmetry of 47%, 94%, and 99% of the semi-span $b/2$. The four inboard dye ports were located at a distance of 1 mm from the leading edge of the wing, and the two outboard ports, which were essentially coincident with the tip of the wing, were at a distance of 10 mm from the leading edge. Side and plan views of the visualized patterns of the flow were recorded simultaneously using two CCD cameras. Experiments were performed at free-stream velocities of $U = 45$ and 90 mm/s, giving Reynolds numbers based on chord of $\mathrm{Re} = 5000$ and 10 000.

The facility at the US Air Force Laboratory (AFRL) is a free-surface water tunnel of 4:1 contraction and 46 cm wide by 61 cm high test-section, with turbulence intensity estimated at 0.4%, and a surface skimmer to damp sloshing. The tunnel is fitted with a three degree of freedom electric rig, enabling independent control of pitch or rotation, plunge or heave, and "surge" or streamwise-aligned translation. The rig is controlled through a Galil DMC 4040 Ethernet controller. Pitch and plunge are made possible by a pair of motors mounted vertically on a plate above the tunnel test-section. Each motor actuates a vertical "plunge rod", which connects via a bushing to a coupler piece. The upstream plunge rod is constrained to move purely vertically, whereas the downstream plunge rod is allowed to swing in the test-section vertical plane of symmetry. The pitch pivot point can be varied by suitable choices of phase and amplitude difference in trajectory of the two vertically mounted motors. For all cases where the pitch pivot point is not coincident with the bushed end of the front plunge rod, there will be a parasitic streamwise displacement of the model. This is removed using the third degree of freedom, surge, using a larger linear motor mounted horizontally aft of the pitch–plunge carriage.

The model is a carbon-fiber plate of nominally 3 mm thickness, 234 mm span, and 117 mm chord and rounded (semicircular) edges. It was supported by an aft-mount sting with nominal diameter of $0.085C$; in essence, this sting was an extension of the trailing edge of the plate, which was centered at the plane of symmetry of the plate. Dye is injected from four 0.5 mm diameter steel-tube probes running along the model surface and exiting at the leading edge, firing in the spanwise direction. The probes exiting at the spanwise centerplane and the spanwise 87.5% plane are mounted along the model's pressure side. Two other probes, exiting at the spanwise 75% plane and the 97.5% spanwise location (6 mm away from the wingtip), are mounted along the model's suction side. All probes connect to a plenum fed through a common syringe, actuated by a programmable pump set to 1 mL/min infusion volumetric rate. The ratio of dye firing speed to free-stream speed is approximately 0.3. Evidence that such firing speeds are nonintrusive is that turning the dye off, and repeating the plate motion with residual pressure in the dye lines, shows no discernable change in the visualized flow pattern, other than of course reduction in image contrast. The dye consists approximately of 60% blue food coloring, 20% rubbing alcohol, and 20% "half and half" cream, by volume. The nominal Reynolds number of the experiment was 10 000, at a tunnel free-stream speed of 85 mm/s, in water at 21 °C. Test-section geometric blockage at the maximum angle of attack is 6.3%, based on the model's projected frontal area.

The wing (plate) motion in both laboratories is shown in Fig. 1(b). The pitching motion is a linear pitch-up and pitch-down sequence, followed by a hold on returning to zero angle of attack, with smoothing (nonzero acceleration) at the motion extrema to avoid structural excitations. Plunging motion induces an effective instantaneous angle of attack θ_{eq} from the arctangent of the ratio of plunge speed to the free-stream. As shown in Eq. (1), this can be set equal to instantaneous incidence angle θ of a pitching motion:

$$\arctan\left(\frac{\dot{h}(t)}{U_\infty}\right) = \theta_{\mathrm{eq}}(t) \equiv \theta \tag{1}$$

Therefore, at a given value of time $t = C/U$ in the schematic of Fig. 1, $\theta_{\mathrm{eq}} = \theta$.

3. Results

3.1. Patterns of leading-edge vortex formation for pitch about the quarter chord

Fig. 2(a) directly compares the development of the flow patterns using two different visualization techniques. Images in the left column are at $\mathrm{Re} = 5000$, and in the right column, at $\mathrm{Re} = 10\,000$. Each data set shows side and plan views.

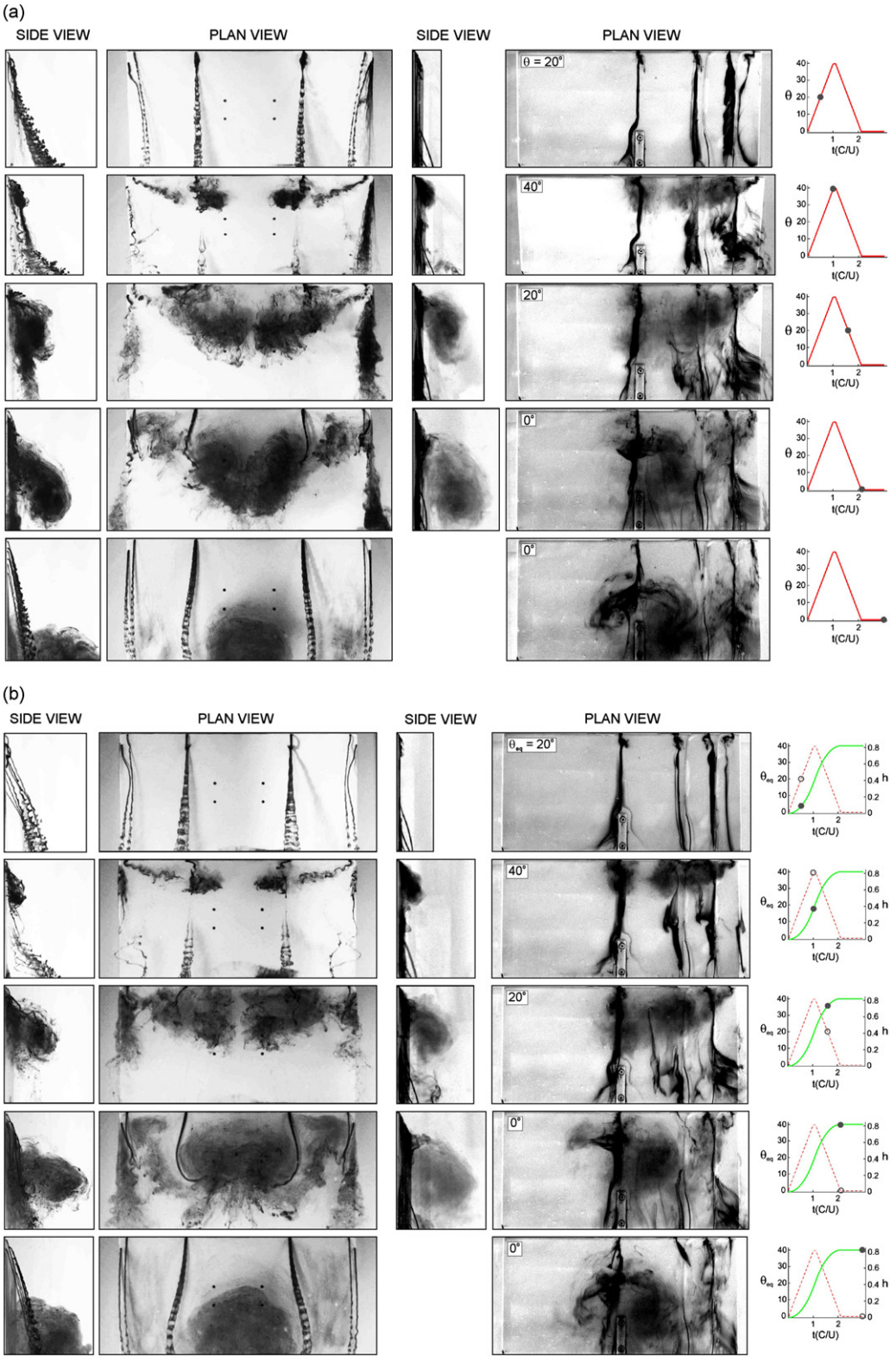

Fig. 2. (a) Side and plan views of onset and development of vortex structure during pitch-up–pitch-down motion using dye visualization at LU (left column, Re = 5000) and AFRL (right column, Re = 10000). Pitch point $x_p/C = 0.25$ and $K = 0.35$. (b) Side and plan views of onset and development of vortex structure during plunging motion using dye visualization at LU (left column, Re = 5000) and at AFRL (right column, Re = 10000). Pitch point $x_p/C = 0.25$ and $K = 0.35$.

The instantaneous angle of attack is indicated by the dot on the schematic of the pitching schedule (θ versus time t) given in the right column.

In the first row of images of Fig. 2(a), corresponding to $\theta = 20^\circ$ on the upstroke, both the side and plan views indicate lack of detectable formation of a leading-edge vortex. Subsequently, at $\theta = 40^\circ$, as indicated in the second row of images, a small vortex is evident in the side views. The corresponding plan views show inboard-oriented axial flow through the center of the leading-edge vortex towards the plane of symmetry of the wing. In the third row of images, at $\theta = 20^\circ$ on the downstroke, the side view of the leading-edge vortex shows a substantial increase in scale and, correspondingly, the plan view shows that the pattern of axial flow through the leading-edge vortex has reached the plane of symmetry. At the end of the downstroke, $\theta = 0^\circ$, in the fourth row of images, the three-dimensional vortex has matured to a larger scale and undergone substantial distortion, evident in both the plan and side views. Finally, in the fifth row of images, the dye marking the large-scale vortex has evolved to a confined cluster concentrated at the plane of symmetry of the wing, which suggests that vorticity marked by the dye during the earlier stages of formation now resides in that region as well. The plan view image in the fifth row, right column, shows extension of the dye marker to further upstream locations than the corresponding image in the left column, apparently due to the continuous injection of dye along the plane of symmetry and, perhaps, an influence of the sting extension from the trailing edge. Generally speaking, however, for all of the images in the right column at $\mathrm{Re} = 10\,000$ versus the left column (at $\mathrm{Re} = 5000$) of Fig. 2(a), the patterns are quite similar, thereby suggesting an insignificant influence of Reynolds number in this range. Differences can be ascribed to intensity of the dye injection, that is, the extent to which the dye flow itself is intrusive in the local flowfield. When the flow is instantaneously nearly attached, dye flow intrusion can be significant. But large vortical structures subsume all discernable effects of how the dye happens to be introduced.

The dye patterns of Fig. 2(a) show distinctive stages of flowfield evolution. We now consider the extent to which these patterns persist for variations of pitching axis location and reduced pitch rate, and in comparison of plunge versus pitch.

3.2. Comparison of pitch and plunge

Fig. 2(b) shows images associated with the equivalent pitching motion. The instantaneous vertical displacement h and the equivalent angle of attack θ_{eq} of the plunging motion are indicated, respectively, by filled and open dots on each of the schematics in the right column of Fig. 2(b). Each image in Fig. 2(b) can be directly compared with the image at the corresponding location in Fig. 2(a). In an overall sense, the patterns of Fig. 2(b) are remarkably similar to their counterparts in Fig. 2(a). The onset of vortex formation from the leading edge, characterized by pronounced axial flow at $\theta = 40^\circ$ in Fig. 2(a) and $\theta_{eq} = 40^\circ$ in Fig. 2(b), is nearly indistinguishable. At later times, corresponding to the third–fifth rows of images, the pivot $x_p/C = 0.25$ dye patterns are displaced slightly further in the downstream direction and are somewhat distorted relative to the patterns indicated for the plunge casein the plan views. The side views in the fourth row of images show that the elongated dye cluster is inclined at a shallower angle with respect to the surface of the wing for the pivot $x_p/C = 0.25$ case, relative to the plunge case. All of these features are discernible distinctions that occur along downstream portions of the wing, which are not accounted for in the angle of attack equivalence between these motions. Nevertheless, as shown in the fifth row of images, which represents the end state, the spatial extent and position of the dye cluster concentrated near the trailing edge is quite similar for pivot $x_p/C = 0.25$ and plunge. In summary, the angle of attack equivalence between the pitching and plunging motions yields a strong correlation of the overall form and phase shift of the initial stage of vortex formation for these distinctively different types of wing motion.

Quasi-steady airfoil theory (see for example Leishman, (2000)) predicts that pitch-rate effects on lift coefficient are zero for a three-quarter-chord pivot location, whence perhaps pitch with pivot about this point should be most akin to plunge. We do not consider lift coefficient here, instead focusing on flowfield evolution. And from comparison of the five cases under consideration, qualitatively it appears that the quarter-chord pitch is most akin to plunge.

3.3. Effect of pitch point location and pitch rate

Fig. 3 shows a comparison of pitch pivot point effects. In all cases, $\mathrm{Re} \sim 10\,000$ and $K = C\dot{\theta}/2U_\infty = 0.35$. The pitch pivot point locations are $x_p/C = 0.00$ (leading edge), 0.25, 0.50, 0.75, and 1.00 (trailing edge); plunge is also compared. The leading-edge pivoting case is taken as a reference case, where we consider the flowfield snapshot at the maximum angle of attack; that is, at the top of the pitch ramp. The leading-edge vortex (LEV) occupied approximately the forward third of the wing suction side, and strong inboard flow is seen in the planform view. We assert a flowfield similarity relationship as follows: for a given pitch rate, for any two choices of pivot point location, one can find a

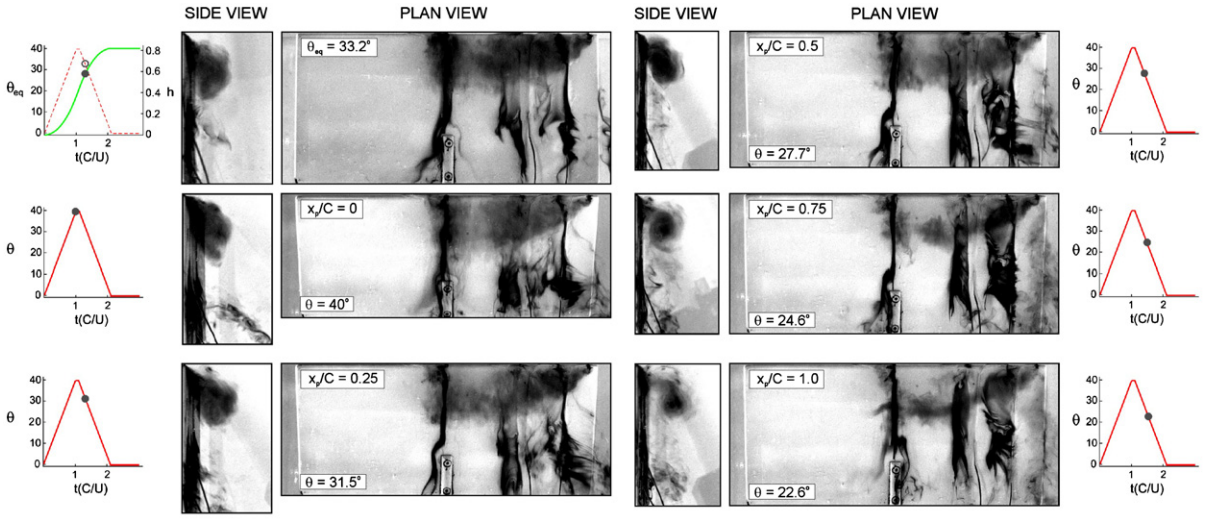

Fig. 3. Side and plan views of AFRL dye injection, Re = 10000, $K = 0.35$. Plunge is represented by the set of images at the top left, followed by pitch pivoting at $x_p/C = 0$, 0.25, 0.5, 0.75, and 1.0.

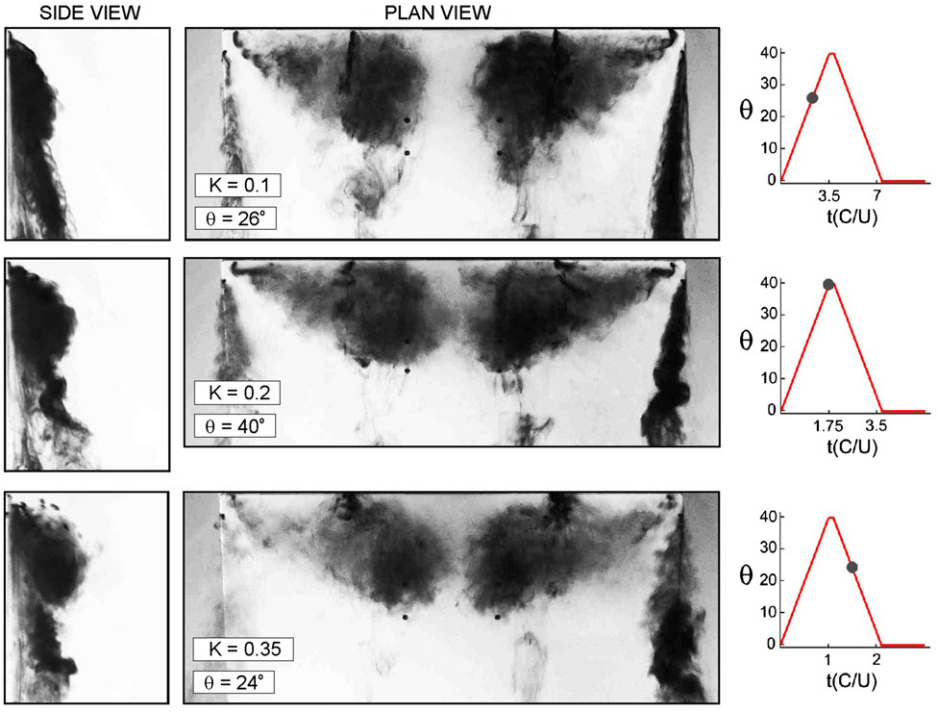

Fig. 4. Side and plan views of LU dye visualization showing effect of magnitude of reduced frequency $K = 0.1$, 0.2, and 0.35 on vortex structure. Pitch pivot point $x_p/C = 0.25$, Re = 10000.

snapshot of motion history for the one and for the other, such that the LEV development will be similar. This does not hold for late in the motion history, long after the pitch ramp peak has been passed. But for quarter-chord pivot, the LEV development in the downstroke at instantaneous incidence angle $\sim 31.5^\circ$ is much akin to that of the leading edge

pivot case at $\theta = 40^\circ$. For half-chord pivot, the relevant instantaneous incidence angle is 27.7° on the downstroke; for three-quarter-chord pivot, it is 24.6°; for trailing-edge pivot, it is 22.6°; and finally, for the plunge, it is 33.2°.

Fig. 4 compares images for a given location of the pitch pivot point $x_p/C = 0.25$, i.e., at quarter chord, for different values of reduced pitch rate $K = C\dot{\theta}/2U_\infty = 0.1$, 0.2, and 0.35. The reference pattern of the LEV development is taken to occur at the maximum angle of attack $\theta = 40^\circ$, i.e., at the top of the pitch motion, for $K = 0.2$. With the hypothesis that the LEV pattern exhibits similarity at different values of K, examination of movies yielded the LEV patterns at the values of angle of attack θ and reduced frequency K indicated in Fig. 4. In essence, the effect of increasing K is to advance occurrence of the LEV pattern to smaller values of C/U, but to delay it along the indicated pitching schedule.

4. Concluding remarks

The major features of the flow structure on an aspect ratio of 2 rectangular wing executing constant-rate pitch-up followed by pitch-down are remarkably similar for variations of pitch point location and reduced frequency extending over the range from $K = 0.1$ to 0.35. Such variations simply induce a shift in time of occurrence of the sequence of three-dimensional flow separation events. This time shift is represented by a reference flow structure, i.e., the three-dimensional form of the leading-edge vortex (LEV), during the late stage of its formation. As the pitch point is moved from the leading to the trailing edge of the wing, the appearance of the LEV is delayed by the order of one-half convective time scale C/U. When the reduced frequency is increased by a factor of 3.5, the LEV is advanced in time by a factor of approximately $2C/U$.

Comparison of pitch and plunge, whereby the equivalent angle of attack of plunge is matched to the angle of attack of pitch, again shows that the sequence of three-dimensional flow events is well correlated at successive times. The flowfield in a plunging maneuver is very similar to that of pitch about the quarter chord.

We find evidence, therefore, of a universality of time scale of flowfield evolution, which can be generalized across a range of motion rates and type of kinematics. It remains to consider whether the history of aerodynamic forces may obey a scaling akin to that of the flowfield.

References

Blondeaux, P., Fornarelli, F., Guglielmini, L., Triantafyllou, M.S., Verzicco, R., 2005. Numerical experiments on flapping foils mimicking fish-like locomotion. Physics of Fluids 17 (11) 113601-1–113601-12.

Buchholz, J.H.J., Smits, A.J., 2006. On the evolution of the wake structure produced by a low-aspect-ratio pitching panel. Journal of Fluid Mechanics 546, 433–443.

Buchholz, J.H.J., Smits, A.J., 2008. The wake structure and thrust performance of a rigid low-aspect-ratio pitching panel. Journal of Fluid Mechanics 603, 331–365.

Cohn, R.K., Koochesfahani, M.M., 1993. Effect of boundary conditions on axial flow in a concentrated vortex core. Physics of Fluids A 5 (1), 280–282.

Dong, H., Mittal, R., Najjar, F.M., 2006. Wake topology and hydrodynamic performance of low-aspect-ratio flapping foils. Journal of Fluid Mechanics 566, 309–343.

Freymuth, P., 1989. Visualizing the connectivity of vortex systems for pitching wings. ASME Journal of Fluids Engineering 111, 217.

Graham, G.M., Yeow, K.F., 1990. The two dimensional post stall maneuver of a NACA 0015 airfoil at high pitching rates. AIAA-1990-2810.

Koochesfahani, M.M., 1989. Vortical patterns in the wake of an oscillating airfoil. AIAA Journal 27 (9), 1200–1205.

Kurosaka, M., Christiansen, W.H., Goodman, J.R., Tirres, L., Wohlman, R.A., 1988. Crossflow transport induced by vortices. AIAA Journal 26, 1403–1405.

Leishman, J.G., 2000. In: Principles of Helicopter Aerodynamics. Cambridge University Press.

Ol, M., McAuliffe, B.R., Hanff, E.S., Scholz, U., Kaehler, Ch., 2005. Comparison of laminar separation bubble measurements on a low Reynolds number airfoil in three facilities. AIAA-2005-5149.

Parker, K., von Ellenrieder, K.D., Soria, J., 2005. Using stereo multi-grid DPIV measurements to investigate the vortical skeleton behind a finite-span flapping wing. Experiments in Fluids 39, 281–298.

Parker, K., von Ellenrieder, K.D., Soria, J., 2007. Morphology of the forced oscillatory flow past a finite-span wing at low Reynolds number. Journal of Fluid Mechanics 571, 327–357.

Taira, K., Colonius, T., 2009a. Three-dimensional flows around low-aspect-ratio flat-plate wings at low Reynolds numbers. Journal of Fluid Mechanics 623, 187–207.

Taira, K., Colonius, T., 2009b. Effect of tip vortices in low-Reynolds number post stall flow control. AIAA Journal 47 (3), 749–756.

Visbal, M., Gogineni, S., Gaitonde, D., 1998. Direct numerical simulation of a forced transitional plane wall jet. AIAA Paper 98-2643, June, 29th AIAA Fluid Dynamics Conference, Albuquerque, NM, USA.

Von Ellenrieder, K.D., Parker, K., Soria, J., 2003. Flow structures behind a heaving and pitching finite-span wing. Journal of Fluid Mechanics 490, 129–138.

Yilmaz, T., Rockwell, D., 2010. Three-dimensional flow structure on a maneuvering wing. Experiments in Fluids 48, 539–544.